

Quantum Oscillations and Magnetic Reconstruction in the Delafossite PdCrO_2

Clifford W. Hicks,^{1,2} Alexandra S. Gibbs,^{1,3,4} Lishan Zhao,^{1,2} Pallavi Kushwaha,² Horst Borrmann,² Andrew P. Mackenzie,^{1,2,*} Hiroshi Takatsu,⁵ Shingo Yonezawa,⁶ Yoshiteru Maeno,⁶ and Edward A. Yelland^{1,7}

¹*Scottish Universities Physics Alliance (SUPA), School of Physics and Astronomy,
University of St Andrews, St Andrews KY16 9SS, United Kingdom*

²*Max Planck Institute for Chemical Physics of Solids, Nöthnitzer Str. 40, 01187 Dresden, Germany*

³*School of Chemistry and EaStCHEM, University of St Andrews,
North Haugh, St Andrews KY16 9ST, United Kingdom*

⁴*Max Planck Institute for Solid State Research, Heisenbergstrasse 1, 70569 Stuttgart, Germany*

⁵*Department of Physics, Tokyo Metropolitan University, Tokyo 192-0397, Japan*

⁶*Department of Physics, Graduate School of Science, Kyoto University, Kyoto 606-8502, Japan*

⁷*SUPA, School of Physics and Astronomy, and Centre for Science at Extreme Conditions,
University of Edinburgh, Mayfield Road, Edinburgh EH9 3JZ, United Kingdom*

(Dated: 9 Apr 2015)

We report quantum oscillation data on the metallic triangular antiferromagnet PdCrO_2 . We find that, to very high accuracy, the observed frequencies of PdCrO_2 can be reproduced by reconstruction of the (nonmagnetic) PdCoO_2 Fermi surface into a reduced zone. The reduced zone corresponds to a magnetic cell containing six chromium sites, giving a $\sqrt{3} \times \sqrt{3}$ in-plane reconstruction, and $\times 2$ interplane reconstruction. The interplane ordering represents a reduction in lattice symmetry, possibly to monoclinic, and an associated lattice distortion is expected. In addition, we report a magnetic transition under an applied in-plane field that is probably equivalent to the spin-flop transition reported for CuCrO_2 , and present data on its field-angle dependence. We also report measurements of the resistivity of PdCrO_2 up to 500 K.

PACS numbers:

Magnetic ions coordinated on a triangular lattice of ten yield interesting magnetic properties. A prominent example is the insulating CrO_2 sheet, stabilised in materials like LiCrO_2 and PdCrO_2 . In these compounds, the Cr formal charge is +3, and its configuration is $3d^3$. The crystal field at the Cr sites is nearly octahedral, inducing a gap between the quasi- t_{2g} (d_{xy} , d_{xz} , and d_{yz}) and quasi- e_g ($d_{3z^2-r^2}$ and $d_{x^2-y^2}$) bands. The quasi- t_{2g} levels are therefore half-filled, and the CrO_2 sheet is a Mott insulator: strong Hund's rule coupling aligns the spins on each Cr site, giving a total spin on each Cr site of nearly $3/2$. The CrO_2 sheet is a Heisenberg system, that orders at low temperatures into the 120° triangular Néel phase.

Of materials containing such a CrO_2 sheet, AgCrO_2 , CuCrO_2 , and PdCrO_2 have the delafossite crystal structure, while LiCrO_2 , NaCrO_2 , and KCrO_2 have the closely-related ordered rock salt structure. All of these systems show 120° order, with the Néel temperature depending strongly on the Cr-Cr spacing. The ordered rock salt structure gives substantially smaller interplane spacings than the delafossite structure, and somewhat higher Néel temperatures. [1]

The interlayer order is a more subtle problem than the intralayer order: in all of these systems the Cr sheets are stacked rhombohedrally, so the molecular fields from first- and second-neighbouring layers cancel. However the interlayer order has observable consequences: AgCrO_2 and CuCrO_2 show spin-driven ferroelectricity, while NaCrO_2 and LiCrO_2 do not. [2] AgCrO_2 and

CuCrO_2 have the delafossite structure and NaCrO_2 and LiCrO_2 the ordered rock salt structure, but the more essential difference appears to be the interlayer order: in AgCrO_2 [3] and CuCrO_2 [4, 5], the interlayer ordering is ferroic, in that the vector chirality, the rotational sense of the spin helices that comprise the 120° phase, is the same in all layers. In LiCrO_2 , in contrast, neutron scattering data suggest that the vector chirality alternates from layer to layer [6], while the interplane order of NaCrO_2 is not clear. [7]

This paper focuses on PdCrO_2 . The Néel temperature of PdCrO_2 is $T_N = 37.5$ K, and, like LiCrO_2 , the vector chirality probably alternates from layer to layer, [1, 18] so this feature is not restricted to the ordered rock salt structure.

Whereas the other compounds discussed above are insulators, PdCrO_2 is a metal, due to $4d/5s$ conduction in the Pd sheets. The isostructural, nonmagnetic compound PdCoO_2 also has these Pd sheets, and its carrier mobility was found to exceed that of copper. [15] PdCrO_2 therefore is an interesting system, comprised of highly-conducting sheets interleaved with Mott insulating spacer layers. It would be interesting to determine whether the metallic Pd conduction has any effect on the magnetic order.

What is certainly true is that the Pd conduction can be used as a probe of the magnetic order. Quantum oscillation [9] and angle-resolved photoemission spectroscopy (ARPES) [10, 11] studies have shown that the PdCrO_2 Fermi surfaces result from reconstruction of the PdCoO_2

Fermi surface into the magnetic zone. Observation of an unconventional anomalous Hall effect in PdCrO_2 indicates further that the Cr spins are not co-planar. [12]

In this paper we present measurements of quantum oscillations in PdCrO_2 , and confirm the overall frequencies reported in Ref. [9]. We add greater resolution and a careful comparison with the nonmagnetic PdCoO_2 Fermi surface: we show that reconstruction of the PdCoO_2 Fermi surface reproduces most of the observed oscillation frequencies to very high accuracy; the PdCrO_2 frequencies can be analyzed in detail without recourse to density functional theory calculations. We show that the magnetic coupling is k_z -dependent: it is much weaker at $k_z = \pm\pi$ than at $k_z = 0$. Also, the dominant magnetic scattering vectors are those corresponding to a 6-Cr magnetic unit cell giving a $\times 2$ interplane reconstruction in addition to the $\sqrt{3} \times \sqrt{3}$ in-plane reconstruction. The interplane order represents a reduction in lattice symmetry, from $R\bar{3}m$ (rhombohedral) to, in the highest-symmetry case, $C2/c$ (monoclinic).

We also report a magnetic transition under applied field, at a similar field to a spin flop transition reported in CuCrO_2 , that was observed in the course of measurement of the oscillations. Finally, we present measurements of the resistivity of PdCrO_2 to high temperatures.

METHODS

Single crystals of PdCrO_2 were grown by a NaCl flux method, using PdCrO_2 powder synthesized via a solid-state reaction. [13] We measured magnetic oscillations in two samples of PdCrO_2 , by torque magnetometry, using the same piezoresistive AFM cantilevers as in our previous study on PdCoO_2 . [15, 16] The cantilevers were mounted on rotatable platforms with integrated field angle sensors.

Sample #1 was roughly $230 \times 300 \times 11 \mu\text{m}$, and sample #2 $160 \times 100 \times 15 \mu\text{m}$. For sample #1 the field was rotated about a $\langle 1000 \rangle$ axis (using hexagonal indexing), and for sample #2 a $\langle 1\bar{1}00 \rangle$ axis; these axes are illustrated at the bottom right of Fig. 2. Some raw data for sample #1 are shown in Fig. 1. Low-frequency oscillations (~ 800 T for field angle $\theta \rightarrow 0$) dominate the data. At 0.7 K, these oscillations were discernible at fields as low as 2 T. At high fields (above ~ 10 T), the oscillation amplitude was very large, leading to strong torque interaction: the oscillations had a triangular form, and strong sum and difference frequencies appeared in the Fourier transforms. While torque interaction complicates the analysis somewhat, it may be difficult to avoid if the samples are to be large enough for higher-frequency oscillations to be resolved.

The oscillation amplitudes were history-dependent. Cooling the sample through T_N in a 15 T field resulted in oscillation amplitudes for the α , β , and γ orbits roughly

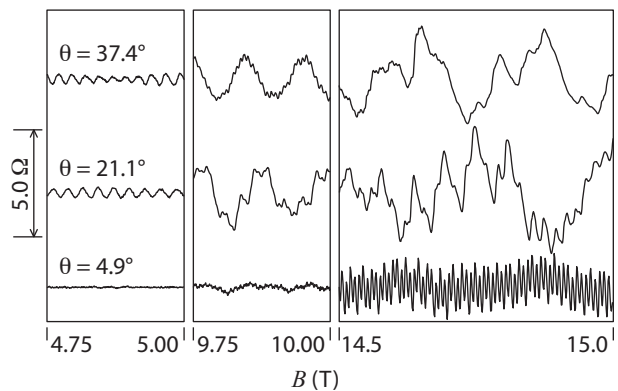


FIG. 1: Magnetic oscillations in sample #1 at three field angles. The y -scale is the resistance of the piezoresistive sense element on the cantilever.

four times as large as with zero-field cooling. These large amplitudes persisted as long as the field was maintained. Releasing the field and heating the sample to ~ 1 K caused the amplitudes to decrease, and re-applying fields up to 15 T did not recover the large amplitudes. The system therefore appears to be nonergodic. A possible origin of glassy behaviour is domain-boundary Cr spins: the relatively large magnetic unit cell of PdCrO_2 means that a complex domain structure is likely.

For measurement of the temperature dependence of the oscillation amplitudes, we cooled the sample in a field and kept the field above 8 T at all times, to maintain large oscillation amplitudes. For measurement of the angle dependence of the frequencies, torque interaction was a greater concern, and the sample was cooled through T_N in zero field. [28]

RESULTS: THE OSCILLATIONS

The oscillation frequencies as a function of field angle are shown in Fig. 2. Four sets of intrinsic peaks can be identified, located, at $\theta = 0$, at around 0.8, 3.5, 10.5, and 27.4 kT. Following Ref. [9], we label these α , β , γ , and δ . All the frequencies scale broadly as $1/\cos(\theta)$, indicating that the Fermi surfaces are highly two-dimensional.

It has been established that the PdCrO_2 orbits result from a $\sqrt{3} \times \sqrt{3}$ reconstruction of the PdCoO_2 Fermi surface, due to the 120° Néel order. [9, 11] This reconstruction is illustrated in Fig. 3. The α and γ orbits are fully reconstructed orbits, while β and δ result from magnetic breakdown, *i.e.* the orbits cross gaps in k -space.

The cyclotron masses were determined for sample #1 by Lifshitz-Kosevich fits to the temperature dependence of the amplitudes. We analysed the data between 7.5 and 11.5 T, avoiding higher fields where torque interaction was very strong, and verified that within this range there was no systematic variation of the masses with field.

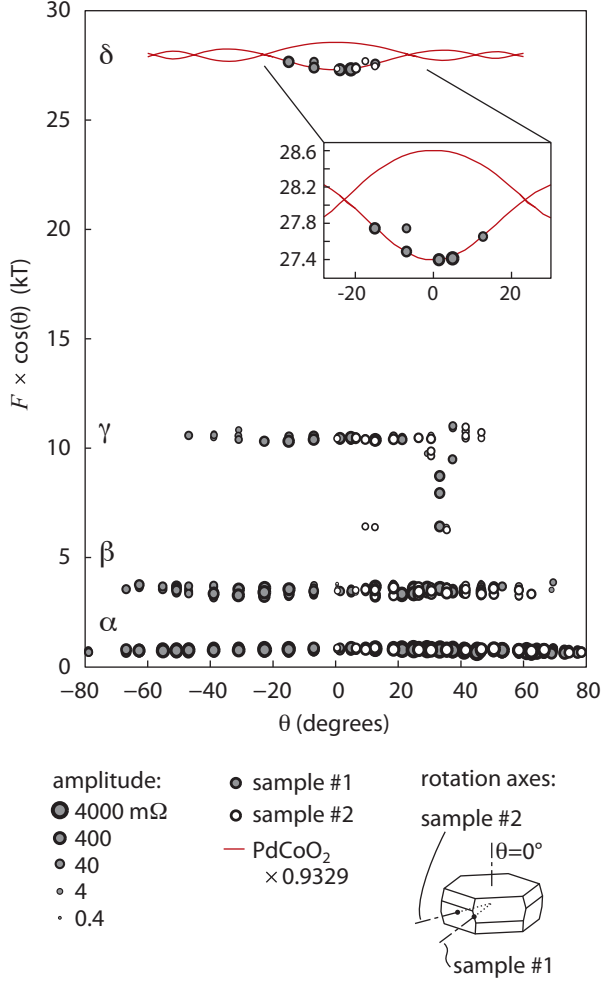


FIG. 2: The observed oscillation frequencies of PdCrO₂, multiplied by $\cos(\theta)$, against field angle θ . The field rotation axes are shown at bottom right, referenced to the nonmagnetic zone. The frequencies are from Fourier transformation of the data over the range 4.2 to 15 T. Frequencies that are clearly sum or difference frequencies are not shown. The indicated amplitudes of the oscillations are the peak-to-peak amplitudes of the oscillations in resistance of the sense element on the cantilever. The PdCoO₂ frequencies are taken from the model in Ref. [15], and have been scaled by 93.3%.

The masses obtained for the α , β , γ , and δ orbits are 0.33 ± 0.01 , 0.84 ± 0.01 , 1.37 ± 0.02 , and $(1.55 \pm 0.04)m_e$, respectively, the fits are shown in the Appendix. These are in good overall agreement with ARPES measurements. A Fermi velocity of 4.2 eV-Å was measured, by ARPES, at the corners of the nonmagnetic Fermi surface, and 4.9 eV-Å at the faces. [11] If an isotropic Fermi velocity of 4.6 eV-Å is taken along the perimeters of the α , β , γ , and δ orbits, masses of 0.34, 0.63, 1.00, and $1.53m_e$ are obtained, respectively: the cyclotron masses from the Lifshitz-Kosevich fits are in very close agreement with the ARPES estimates for α and δ , and $\sim 35\%$ heavier for β and γ . [29]

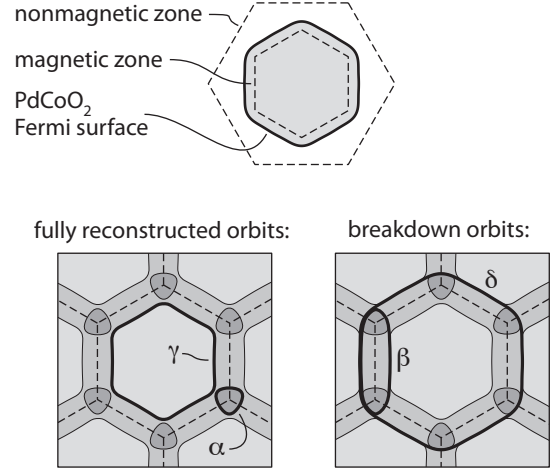


FIG. 3: A two-dimensional model of the reconstruction. Top: the PdCoO₂ Fermi surface in the 2D nonmagnetic zone, and magnetic zone arising from a $\sqrt{3} \times \sqrt{3}$ reconstruction. Bottom: reconstruction into the magnetic zone. The fully reconstructed orbits, α and γ , are illustrated in the left-hand panel, and the breakdown orbits, β and δ , in the right-hand panel.

Also shown in Fig. 2 are the PdCoO₂ frequencies from the parametrised model in Ref. [15], for comparison with PdCrO₂. To make the comparison, the PdCoO₂ frequencies need to be scaled by the square of the ratio of in-plane lattice constants. We found that the best match is obtained with a scaling of 93.3%, which is very close to the expected scaling, $(2.830 \text{ Å}/2.923 \text{ Å})^2 = 93.7\%$. [1, 25]

From the comparison it is apparent that the lower branch of the PdCoO₂ frequencies, arising from the neck orbit (*i.e.* the $k_z = \pm\pi$ orbit), is visible in the PdCrO₂ data, while the upper branch, from the belly orbit ($k_z = 0$), is not. This feature is part of a pattern that extends to the other frequencies: the observed breakdown frequencies derive from reconstruction of the nonmagnetic neck orbit, while the observed fully-reconstructed frequencies derive mainly from the belly orbit. The pattern is illustrated in Table I, which shows the observed PdCrO₂ frequencies (for $\theta \rightarrow 0$) and the expected frequencies based on reconstruction of the PdCoO₂ neck and belly orbits: the neck reconstruction yields the observed β and δ frequencies, and the belly reconstruction α_3 and γ . (The α frequencies comprise three sub-bands, α_1 , α_2 , and α_3 ; we will discuss this in more detail below.)

What this pattern means is that the belly orbit sees the magnetic order more strongly than the neck orbit. This is not surprising: the Cr sites are midway between the Pd sheets (which dominate conduction), and the $k_z = \pm\pi$ Bloch states have zero weight at the planes of the Cr nuclei.

Overall, then, a two-dimensional $\sqrt{3} \times \sqrt{3}$ reconstruction of the PdCoO₂ frequencies, where the reconstruction is weak at $k_z = \pm\pi$, gives a good description of the PdCrO₂ frequencies at $\theta = 0$. We now test the re-

	α_3	β	γ	δ
observed frequencies (kT):	0.87	3.45	10.52	27.40
calc'd $k_z = 0$ freq's (kT):	0.91	3.92	10.50	28.60
calc'd $k_z = \pi$ freq's (kT):	0.69	3.36	11.27	27.40

TABLE I: Observed frequencies at $\theta = 0$, and expected frequencies from two-dimensional $\sqrt{3} \times \sqrt{3}$ reconstruction of the PdCoO_2 $k_z = 0$ and $k_z = \pm\pi$ orbits. Boldface indicates a better match to observations. In the calculations, the PdCoO_2 frequencies are scaled by 93.3%, and avoided crossings at band crossings are neglected apart from their effect on Fermi surface topology.

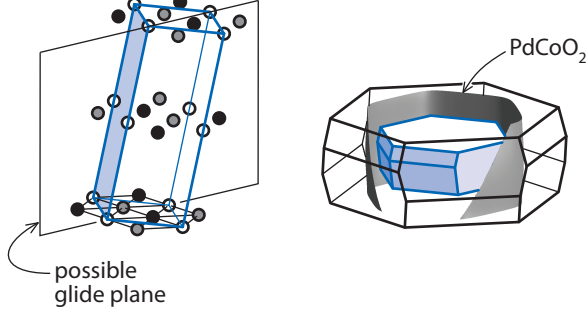


FIG. 4: Left: a possible magnetic cell for PdCrO_2 , that contains 6 Cr sites. The Cr sites are colored black, gray, and white to indicate the three spin directions of each layer. Right: the nonmagnetic first Brillouin zone (black), together with the PdCoO_2 Fermi surface and the 6-site zone, into which the nonmagnetic Fermi surface is reconstructed.

construction at other field angles by performing the full three-dimensional reconstruction.

We first need a three-dimensional magnetic cell. It must contain at least six Cr sites: three per layer to capture the 120° Néel order, and two layers to capture the alternating vector chirality. The cell we test is shown in Fig. 4. [30] The Cr sites are stacked rhombohedrally, so at T_N there are three equivalent choices for the interplane ordering vector. In choosing one of them the lattice symmetry is reduced. The space group of the nonmagnetic lattice is $R\bar{3}m$. The highest-symmetry possible magnetic lattice has space group $C2/c$ (base-centered monoclinic): reflection about the glide plane indicated in Fig. 4 reverses the vector chirality within each layer, and translation along the interplane ordering vector restores the original lattice. [31] Magnetostructural coupling should lead to a lattice distortion associated with the reduction in symmetry, and it is possible that more subtle features in the magnetic order reduce the symmetry further.

The reconstruction is performed as described in textbooks: sections of the nonmagnetic Fermi surface are translated by combinations of reciprocal lattice vectors of the reduced zone until all portions of the original surface are represented within the reduced zone. For our nonmagnetic surface, we take the parametrised model for the

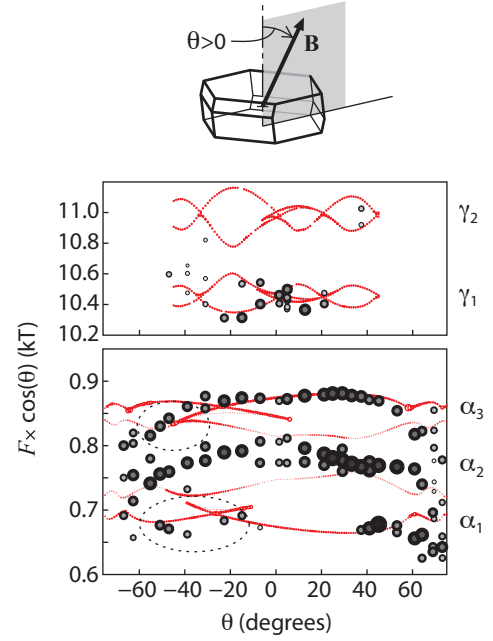


FIG. 5: Red circles: calculated frequencies based on reconstruction of the PdCoO_2 Fermi surface into the magnetic zone shown in Fig. 4. The upper and lower panels show the γ and α frequencies, respectively. In the lower panel, the diameter of the symbols is proportional to the logarithm of the expected oscillation amplitude, based solely on the curvature of the Fermi surfaces. Gray circles: the frequencies observed in sample #1, with the diameter of the symbols proportional to the logarithm of the amplitude.

PdCoO_2 Fermi surface that was determined in Ref. [15]. We do not include finite avoided crossings in our calculation, although the topology of the reconstructed Fermi surfaces is determined by the orientations of the avoided crossings that would occur in the real system. Further details of the calculation are given in the appendix. Our results are shown in Fig. 5, together with the observed frequencies.

There are two γ bands. The lower band, γ_1 , derives from reconstruction of the belly orbit, and γ_2 the neck orbit. γ_2 is not observed in the data because the magnetic coupling is weak for the neck orbit.

Three α bands appear in the data. [32] The lower and upper bands, α_1 and α_3 , are reproduced well by the calculation. α_3 is from the nonmagnetic belly orbit and α_1 the neck orbit, so α_1 has a much lower amplitude in the data. The middle band, α_2 , is not reproduced in the calculations. It could be a breakdown orbit. There are prominent breakdown orbits in the data (β and δ), and the $\times 2$ interplane reconstruction could lead to breakdown orbits that mix segments from the original neck and belly orbits.

For this calculation we supposed that the system chose the interplane ordering vector that aligned the plane of

(possible) glide symmetry with the field rotation plane. The other two possibilities would lead to the glide and rotation planes being separated by 120° . We also calculated this possibility, with the result shown in the Appendix. The match to the data is reasonable but not as good, so it appears that either the glide and rotation planes were aligned by chance, or the fields applied during the measurement re-oriented the magnetic reconstruction.

We also show in the Appendix results for a strictly two-dimensional reconstruction, that would preserve the $R\bar{3}m$ symmetry of the nonmagnetic lattice. The results do not match the data well, and we conclude that the dominant magnetic scattering vectors are those of the magnetic cell shown in Fig. 4.

SPIN FLOP TRANSITION

In addition to quantum oscillations, a large-scale feature appeared during the torque magnetometry measurements on sample #1: a first-order magnetic transition. It occurs at a field of around 6.5 T for $\theta = 90^\circ$ (*i.e.* the field applied in the plane). On the high-field side of the transition the sample has a much larger c -axis magnetic moment than on the low-field side. Fig. 6 shows the set of torque curves obtained in this study, divided by the applied field to yield M_\perp , the magnetisation perpendicular to the applied field, and smoothed so as to exclude the oscillations and show the broad-scale features. The transition and its hysteresis are readily apparent, at $\theta \sim 90^\circ$. It appeared for sample #1 but not #2, so it is sensitive to the direction of the applied field.

Over a small angle range, quantum oscillations were visible both below and above the transition; the Fourier transforms are shown in the Appendix. At each angle within this range, the oscillations have a lower amplitude on the high-field side of the transition than on the low-field side, and the dominant peak shifts to a slightly higher frequency. That the transition affects the oscillations in a consistent manner shows that it is a bulk property.

This transition is at a similar field to a spin-flop transition reported for CuCrO_2 , [22] 5.3 T for temperatures well below T_N , and probably has the same origin. In CuCrO_2 , it has been found by single-crystal neutron diffraction that the spins lie in a $\langle 0001 \rangle - \langle 1\bar{1}00 \rangle$ plane. [5, 23, 24] The transition occurs when the field is applied in a $\langle 1\bar{1}00 \rangle$ direction, but there is no transition for fields applied in a $\langle 1000 \rangle$ direction. It has been shown by symmetry arguments [22] and by direct observation [23] that the transition is a spin flop, where the spin plane rotates by 90° .

For PdCrO_2 , although observation of an unconventional anomalous Hall effect shows that the spins are not co-planar, neutron scattering data show that the spins lie approximately in a $\langle 0001 \rangle - \langle 1\bar{1}00 \rangle$ plane, similar to

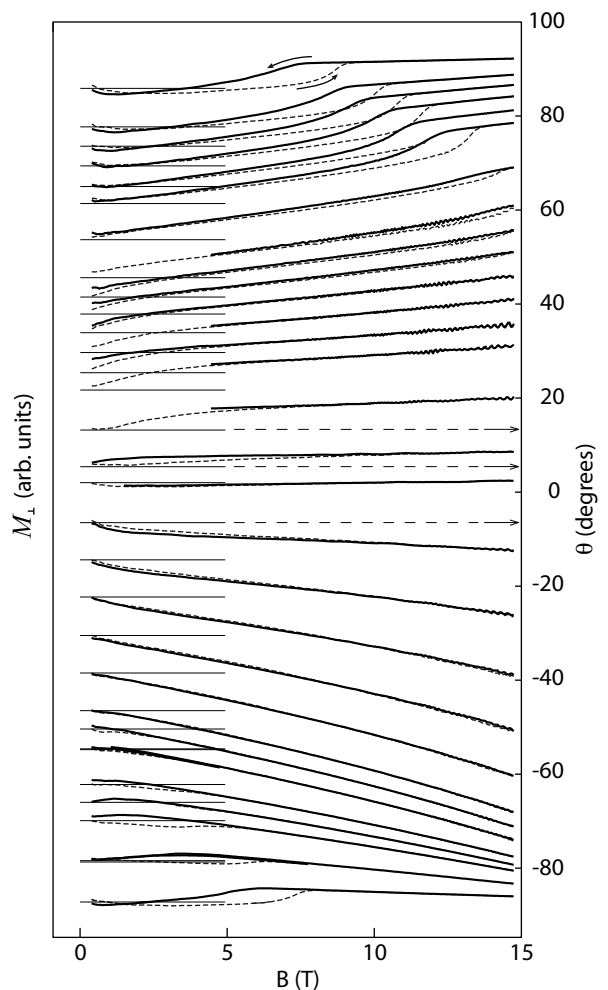


FIG. 6: Perpendicular magnetisation against applied field at 0.7 K, for sample #1, where the field was rotated in a $\langle 0001 \rangle$ - $\langle 1\bar{1}00 \rangle$ plane. Each curve is offset by the field angle θ ; the offsets are indicated by the thin horizontal lines at the left and the angle scale is on the right. The solid lines show downward field sweeps, the dashed lines upward.

CuCrO_2 . Furthermore, and also as in CuCrO_2 , the transition occurs when the field is applied in a $\langle 1\bar{1}00 \rangle$ direction (sample #1), but not in a $\langle 1000 \rangle$ direction (#2). Therefore the transition is probably the same spin flop.

RESISTIVITY

PdCoO_2 has been used as a nonmagnetic analogue of PdCrO_2 in order to extract the magnetic contribution to the specific heat and electrical resistivity. [14, 18] We have shown here that it is a very good comparison: the PdCoO_2 Fermi surfaces are, to high precision, a reconstruction of the PdCrO_2 Fermi surface, and the cyclotron masses match closely: $(1.55 \pm 0.04)m_e$ for the δ orbit of PdCrO_2 , against $1.45 \pm 0.05m_e$ for the (equivalent) neck

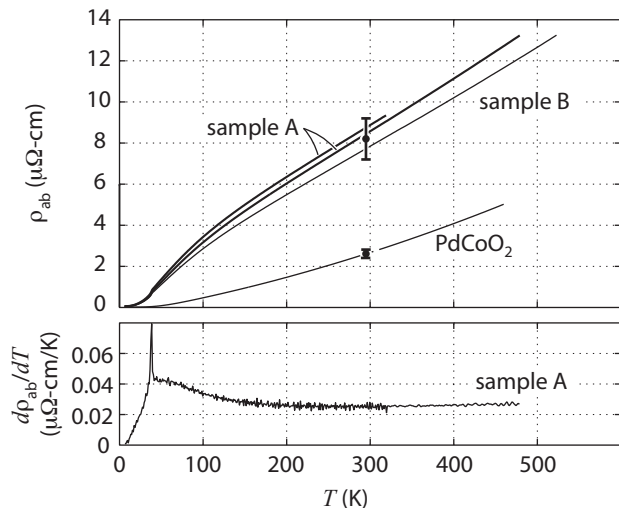


FIG. 7: The resistivity of PdCrO₂ against temperature, for two samples. Sample A had two pairs of voltage contacts. The point at 295 K, with error bars, indicates the room-temperature resistivity: $8.2 \pm 1.0 \mu\Omega\text{-cm}$. Data on a PdCoO₂ sample are also shown, scaled to the room-temperature resistivity determined in Ref. [15]: $2.6 \pm 0.2 \mu\Omega\text{-cm}$. Bottom panel: $d\rho/dT$ for sample A.

orbit of PdCoO₂. [15] The in-plane resistivity of PdCoO₂ is substantially non-linear between ~ 100 and 500 K, a feature attributed to prominent optical phonons. [25] The resistivity of PtCoO₂ also shows this feature. [26] We include in this paper data on the resistivity of PdCrO₂ up to 500 K, in order to extend the comparison reported in Ref. [14] to higher temperatures and to see whether the same feature appears in PdCrO₂.

All samples for resistivity measurement were cut with a wire saw into bars of nearly constant width and thickness, and with length-to-width ratios of ~ 10 , to reduce geometrical uncertainties in conversion of resistance to resistivity. Our data are plotted in Fig. 7. We measured one PdCoO₂ and two PdCrO₂ samples, labelled A and B; sample A had two pairs of voltage contacts, so in total three PdCrO₂ curves were recorded. Averaging the three measurements, the room temperature (295 K) resistivity of PdCrO₂ was found to be $8.2 \pm 1.0 \mu\Omega\text{-cm}$, where the uncertainty is from uncertainty in the sample dimensions. This is in good agreement with that reported in Ref. [14] ($9.4 \mu\Omega\text{-cm}$).

The form of the resistivity of PdCrO₂ is well-established. There is a sharp cusp at T_N , and above T_N the magnetic component of the resistivity, ρ_m , remains well below its saturation value due to short-range correlation. The increase and eventual saturation of ρ_m as the temperature increases leads to a convex temperature dependence of the resistivity.

The in-plane resistivity of PdCrO₂, in contrast to PdCoO₂ and PtCoO₂, is essentially linear from ~ 200 to at least 500 K. It may be that the temperature depen-

dence of ρ_m obscures an optical phonon contribution. ρ_m is expected to saturate when the Cr spins become completely uncorrelated. If ρ_m is estimated by subtracting the resistivity of PdCoO₂ from that of PdCrO₂, then our data indicate that ρ_m continues to increase at temperatures well above room temperature, *i.e.* ρ_m continues to evolve to temperatures an order of magnitude greater than T_N . The Weiss temperature of PdCrO₂ is ~ 500 K, [18] so correlations between the Cr spins are expected to persist to temperatures up to ~ 500 K, and a high saturation temperature of ρ_m may be expected.

DISCUSSION AND CONCLUSION

The quantum oscillation frequencies indicate that the dominant magnetic scattering vectors are those of a six-site magnetic cell with lower symmetry than the nonmagnetic lattice. An associated lattice distortion is expected to onset at T_N . It has been looked for by both neutron and X-ray diffraction, and not found, [1] so any distortion must be small.

The distortion, if it occurs, should resemble that observed in CuCrO₂; [19] there is also evidence for a lattice distortion in AgCrO₂. [21] In CuCrO₂, the vector chirality is the same in each layer and the magnetic cell contains three sites. [2, 4, 5] The magnetic transition is split into two, [20] which is expected for easy-axis-type 120° antiferromagnetism: spins first order along the easy axis, then, at a lower temperature, along an in-plane axis. Ultrasound velocity measurements show that the lattice distortion starts at the upper transition, with no apparent anomaly at the lower transition. [20].

The transition of PdCrO₂ may also be split, although if so the splitting is very small and not generally observed in experiment. [1] Either way, the magnetic order implies two separate reductions in symmetry from $R\bar{3}m$: the choice of interplane ordering vector at the (possible) upper transition, and the choice of spin plane at the lower transition (where, again, in PdCrO₂ the spins are only approximately co-planar). The two symmetry reductions are likely to couple. The ultrasound data on CuCrO₂ suggest that in that system it is the interplane ordering vector that more strongly drives the distortion.

The angle dependence of the spin-flop transition in PdCrO₂ is interesting: the transition field appears to vary smoothly from ~ 15 T on one side of the plane (at $\theta \sim +55^\circ$) to nearly zero on the other (at $\theta \sim -55^\circ$). At $B = 0$, however, the field angle is a meaningless parameter, so if there is in fact an endpoint near $B = 0$ then the high- and low-field states are adiabatically connected to each other. Whether this is true and how it might occur for a 90° spin flop requires further investigation.

In summary, PdCrO₂ is an interesting system comprised of alternating highly-conductive sheets and Mott-insulating spacer layers. It provides a good model for

study of the interaction between metallic conduction and antiferromagnetic order: the conduction is well-characterized, arising from a single, open Fermi surface, and much is known about the magnetic order. Also, there are related compounds that permit precise comparisons, such as the nonmagnetic PdCoO_2 , and other CrO_2 -based delafossite and ordered rock salt materials. Several avenues of inquiry remain open.

We acknowledge useful discussions with John W. Allen, Christopher A. Hooley, Peter Thalmeier, and Burkhardt Schmidt, and practical assistance from Nabhanila Nandi. We acknowledge funding from the UK EPSRC, the MEXT KAKENHI (No. 21340100), the Royal Society, the Wolfson Foundation, and the Max Planck Society.

* Electronic address: apm9@st-andrews.ac.uk

- [1] H. Takatsu, G. Nénert, H. Kadowaki, H. Yoshizawa, M. Enderle, S. Yonezawa, Y. Maeno, J. Kim, N. Tsuji, M. Takata, Y. Zhao, M. Green, and C. Broholm, *Phys. Rev. B* **89** 104408 (2014).
- [2] S. Seki, Y. Onose, Y. Tokura, *Phys. Rev. Lett.* **101** 067204 (2008).
- [3] Y. Oohara, S. Mitsuda, H. Yoshizawa, N. Yaguchi, H. Kuriyama, T. Asano, and M. Mekata, *J. Phys. Soc. Japan* **63** 847 (1994).
- [4] H. Kadowaki, H. Kikuchi, and Y. Ajiro, *J. Phys.: Condens. Matter* **2** 4485 (1990).
- [5] M. Frontzek, G. Ehlers, A. Podlesnyak, H. Cao, M. Matsuda, O. Zaharko, N. Aliouane, S. Barilo, and S.V. Shiryayev, *J. Phys.: Condensed Matter* **24** 016004 (2012).
- [6] H. Kadowaki, H. Takei, and K. Motoya, *J. Phys.: Condens. Matter* **7** 6869 (1995).
- [7] D. Hsieh, D. Qian, R.F. Berger, R.J. Cava, J.W. Lynn, Q. Huang, and M.Z. Hasan, *Physica B* **403** (2008) 1341.
- [8] A.I. Coldea *et al*, *Phys. Rev. B* **90** 020401R (2014).
- [9] Jong Mok Ok, Y. J. Jo, Kyoo Kim, T. Shishidou, E. S. Choi, Han-Jin Noh, T. Oguchi, B. I. Min, and Jun Sung Kim, *Phys. Rev. Lett.* **111** 176405 (2013).
- [10] J. A. Sobota, K. Kim, H. Takatsu, M. Hashimoto, S.-K. Mo, Z. Hussain, T. Oguchi, T. Shishidou, Y. Maeno, B. I. Min, and Z.-X. Shen, *Phys. Rev. B* **88** 125109 (2013).
- [11] Han-Jin Noh, Jinwon Jeong, Bin Chang, Dahee Jeong, Hyun Sook Moon, En-Jin Cho, Jong Mok Ok, Jun Sung Kim, Kyoo Kim, B. I. Min, Han-Koo Lee, Jae-Young Kim, Byeong-Gyu Park, Hyeong-Do Kim, and Seongsu Lee, *Sci. Reports* **4** 3680 (2014).
- [12] H. Takatsu, S. Yonezawa, S. Fujimoto, and Y. Maeno, *Phys. Rev. Lett.* **105** 137201 (2010).
- [13] H. Takatsu and Y. Maeno, *J. Cryst. Growth* **312** 3461 (2010).
- [14] H. Takatsu, S. Yonezawa, C. Michioka, K. Yoshimura, and Y. Maeno, *J. Phys.: Conference Series* **200** 012198 (2010).
- [15] C.W. Hicks, A.S. Gibbs, A.P. Mackenzie, H. Takatsu, Y. Maeno, and E.A. Yelland, *Phys. Rev. Lett.* **109** 116401 (2012).
- [16] The cantilevers are model PRC120, from Seiko Precision Instruments. The sense element is piezoresistive, and the datasheet lists the response, at room temperature, as $16.5 \text{ } \Omega/\mu\text{m}$. The spring constant is $\approx 40 \text{ N/m}$, and the length $120 \text{ } \mu\text{m}$; these parameters can be combined to yield a response to torque of $\approx 3 \cdot 10^9 \text{ } \Omega/\text{N-m}$.
- [17] R.D. Shannon, D.B. Rogers, and C.T. Prewitt, *Inorganic Chemistry* **10** 713 (1971).
- [18] H. Takatsu, H. Yoshizawa, S. Yonezawa, and Y. Maeno, *Phys. Rev. B* **79** 104424 (2009).
- [19] K. Kimura, T. Otani, H. Nakamura, Y. Wakabayashi, and T. Kimura, *J. Phys. Soc. Japan* **78** 113710 (2009).
- [20] O. Aktas, G. Quirion, T. Otani, and T. Kimura, *Phys. Rev. B* **88** 224104 (2013).
- [21] A.M.L. Lopes, G.N.P. Oliveira, T.M. Mendonça, J. Agostinho Moreira, A. Almeida, J.P. Araújo, V.S. Amaral, and J.G. Correia, *Phys. Rev. B* **84** 014434 (2011).
- [22] K. Kimura, H. Nakamura, S. Kimura, M. Hagiwara, and T. Kimura, *Phys. Rev. Lett.* **103** 107201 (2009).
- [23] M. Soda, K. Kimura, T. Kimura, and K. Hirota, *Phys. Rev. B* **81** 100406R (2010).
- [24] M. Poienar, F. Damay, C. Martin, J. Robert, and S. Petit, *Phys. Rev. B* 104411 (2010).
- [25] H. Takatsu, S. Yonezawa, S. Mouri, S. Nakatsuji, K. Tanaka, and Y. Maeno, *J. Phys. Soc. Japan* **76** 104701 (2007).
- [26] P. Kushwaha, P.J.W. Moll, N. Nandi, and A.P. Mackenzie, arXiv:1411.6162.
- [27] C. Bergemann, A.P. Mackenzie, S.R. Julian, D. Forsythe, and E. Ohmichi, *Advances in Physics* **52** 639 (2003).
- [28] While measuring the angle dependence of the oscillations in sample #1, we performed a “de-Gauss” routine at the start of each run, in which the field was ramped to -2 T , then $+1 \text{ T}$, then -0.5 T , and so on. The aim was to reduce the probability of the system evolving gradually into a more ordered state, with larger oscillation amplitudes, though it is not clear whether the procedure had much effect.
- [29] For calculation of the α and γ expected masses, we use the α_3 and γ_1 orbits.
- [30] In Refs. [6] (LiCrO_2) and [1] (PdCrO_2), single-crystal neutron scattering data are analyzed using an 18-site magnetic cell. This is the smallest that can preserve $R\bar{3}m$ symmetry: to preserve $R\bar{3}m$ symmetry the interplane ordering vector must take on all three possibilities in an ABCABC order, so six layers are required to capture both this and the alternating vector chirality. The resulting most-likely magnetic structure in Ref. [1] can be reduced to a six-site magnetic cell.
- [31] The unit cell shown in Fig. 4 is metrically triclinic — none of the angles are 90° — but if the glide symmetry is preserved then a 12-site monoclinic supercell can be constructed.
- [32] Ok *et al* also identify three α bands. [9] However the frequencies they label α_1 and α_2 are both part of α_2 in our labelling scheme, and Ok *et al* do not resolve the frequency we label α_1 .

APPENDIX

In the Appendix we first present some supplementary data, and then give further details on the calculation of the reconstruction.

Fig. 8 shows the Lifshitz-Kosevich fits to the oscillation amplitudes determined over the field range 8.5–9.5 T. Four such fits were done, over 1 T field ranges starting at 7.5, 8.5, 9.5, and 10.5 T. The masses reported in the main text are the averages of the masses obtained from these fits.

Fig. 9 shows the Fourier transforms of the oscillations above and below the putative spin-flop transition, for the narrow angle range over which oscillations were observed on both sides of the transition. On the high-field side of the transition, the oscillations have lower amplitudes and the main peak a higher frequency. (The reduction in amplitude may not be immediately apparent in the figure, but normally quantum oscillation amplitudes grow rapidly as the field is increased, and the reduction in amplitude is very clear in the raw data.)

We now give further details on the reconstruction. The first step is to determine the misalignment, if any, between the sample and the field angle sensor mounted on the rotator platform. This misalignment is determined, for sample #1, by comparison of the observed δ frequencies and the scaled PdCoO₂ frequencies, shown in Fig. 2. The best match is obtained when a $0.3 \pm 0.2^\circ$ offset is added to the measured field angle. This is our misalignment, and correction for it is incorporated into all plots of sample #1 frequencies presented in this paper.

We take the nonmagnetic Fermi surface to be the parametrised PdCoO₂ Fermi surface that was determined in Ref. [15]. The parameters specifying the Fermi surface are the radius of a circular, cylindrical base Fermi surface, k_{00} , and then the amplitudes of the corrugations on this base. k_{60} , for example, is the amplitude of the hexagonal distortion. k_{01} sets the difference between the radii of the neck and belly orbits. A thorough description of this system of parametrization is given in Ref. [27].

We allow three parameters to be adjusted, within small ranges that are consistent with experiment, to match the overall levels of the observed PdCrO₂ frequencies. We emphasize that this adjustment only tunes the overall

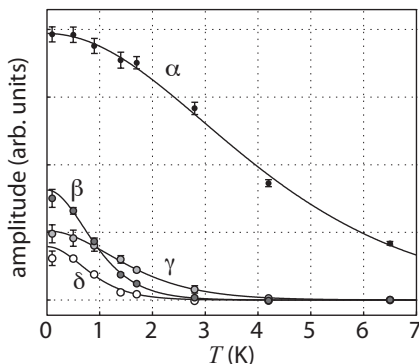


FIG. 8: Lifshitz-Kosevich fits to the amplitudes determined over the field range 8.5–9.5 T.

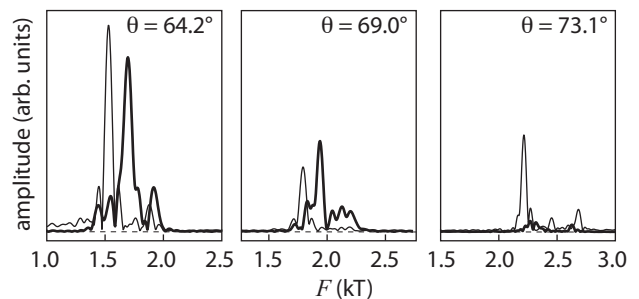


FIG. 9: Fourier transforms of the oscillations below (thin lines) and above (thick lines) the magnetic transition, which at the angles in this figure occurs at $B \sim 10$ T.

levels, and does not substantially alter any of the substructure. These parameters are: (1) The overall size of the Fermi surface (k_{00}), (2) The magnitude of the hexagonal distortion (k_{60}), and (3) the in-plane lattice constant, a . The k_z -dependent Fermi surface corrugations (k_{01} , k_{02} , and k_{31}) are left fixed at the amplitudes found for PdCoO₂. When k_{60} is adjusted, the higher-order amplitudes $k_{12,0}$ and $k_{18,0}$ are adjusted by hand in response, to smooth the faces and sharpen the corners of the Fermi surface so as to match the Fermi surfaces observed by ARPES. [10, 11]

The best match is found with $k_{00} = 0.9219 \text{ \AA}^{-1}$, $k_{60} = 0.036 \text{ \AA}^{-1}$, and $a = 2.927 \text{ \AA}$. Further refinement (for example by allowing a low-temperature lattice distortion, or modification of the k_z -dependent corrugations, or finite avoided crossings) might yield slightly different results—the obtained lattice parameter, for example, is not precisely in line with expectations, as it has been measured to be 2.923 \AA at room temperature and some thermal contraction is expected. [1] But these fitting parameters are within bounds permitted by experiment and are adequate to model the angle dependence.

In addition to the reconstruction shown in the main text, we tested two further possibilities. The first is the same reconstruction but with the other possible orientation relative to the field rotation plane, that the glide plane is rotated from the field rotation plane by 120° . The second tests a hypothetical magnetic zone with vertical side walls, that would preserve the $R\bar{3}m$ symmetry of the nonmagnetic lattice. The results are shown in Fig. 10.

The rotated reconstruction, shown in the left-hand panels in Fig. 10, gives a reasonable match to the data, but not as good as with the glide and rotation planes aligned: it yields the wrong sign on the slope of α_3 against θ , and too low an amplitude on the substructure of the γ_1 frequencies. The $R\bar{3}m$ reconstruction gives a worse match: although it reproduces the α_1 and α_3 frequencies reasonably well, it does not reproduce the structure on γ_1 at all. Therefore, we conclude that the magnetic reconstruction illustrated in Figs. 4 and 5 is the correct

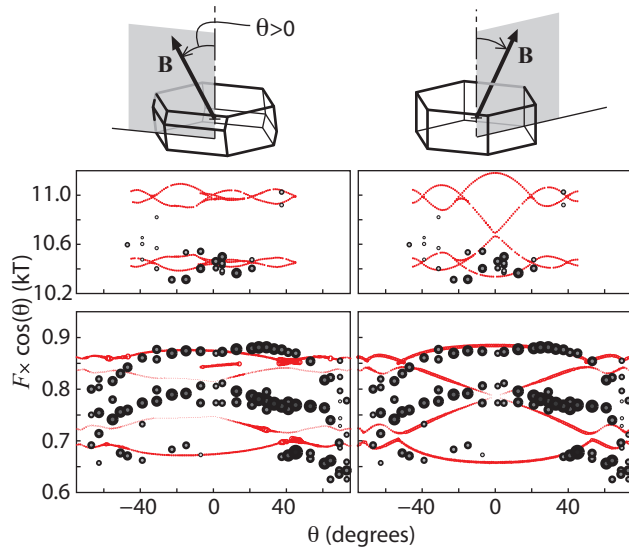


FIG. 10: Oscillation frequency against field angle for two further possibilities for the magnetic reconstruction, discussed in the text.

one.